EuroIntervention 2023;19:612-620 published online ahead of print July 2023

Histological examination of renal nerve distribution, density, and function in humans

Helge Struthoff[1], MD; Lucas Lauder[1]*, MD, Mathias Hohl[1], PhD; Alexander Hermens[1], MD; Abraham Rami Tzafriri[2], PhD; Elazer R. Edelman[3,4], MD, PhD; Michael Kunz[1], MD; Michael Böhm[1], MD; Thomas Tschernig[5], MD; Felix Mahfoud[1], MD, MA

1. Klinik für Innere Medizin III – Kardiologie, Angiologie und Internistische Intensivmedizin, Universitätsklinikum des Saarlandes and Saarland University, Homburg, Germany; 2. CBSET, Inc., Lexington, MA, USA; 3. IMES, Massachusetts Institute of Technology, Cambridge, MA, USA; 4. Division of Cardiovascular Medicine, Brigham and Women's Hospital, Harvard Medical School, Boston, MA, USA; 5. Institute for Anatomy and Cell Biology, Faculty of Medicine, Saarland University, Homburg, Germany

H. Struthoff and L. Lauder contributed equally to this work.

This paper also includes supplementary data published online at: https://eurointervention.pcronline.com/doi/10.4244/EIJ-D-23-00264

KEYWORDS

- hypertension
- renal artery angioplasty
- renal artery stenting
- renal sympathetic denervation

Abstract

Background: Renal denervation is optimised when guided by knowledge of nerve distribution.

Aims: We aimed to assess sympathetic nerve distribution along the renal arteries, especially in post-bifurcation vessel segments.

Methods: Renal arteries and surrounding tissue from 10 body donors were collected and examined histologically. Immunohistochemical staining was used to analyse nerve distribution and to identify afferent and efferent sympathetic nerves.

Results: A total of 6,781 nerves surrounding 18 renal arteries were evaluated. The mean lumen-nerve distance of the left renal artery (2.32±1.95 mm) was slightly greater than the right (2.29±2.03 mm; p=0.161); this varied across the arteries' courses: 3.7±2.3 mm in proximal segments, 2.5±2.0 mm in middle segments, 1.9±1.6 mm in distal prebifurcation segments and 1.3±1.0 mm in post-bifurcation segments (p<0.001). The number of nerves per quadrant was highest in the proximal segments (13.7±18.6), followed by the middle (9.7±7.9), distal prebifurcation (8.0±7.6), and distal post-bifurcation (4.3±4.0) segments (p<0.001). Circumferentially, the number of nerves was highest in the superior (7.8±9.4) and the ventral (7.6±13.1) quadrants (p=0.638). The mean tyrosine hydroxylase (TH) to calcitonin gene-related peptide (CGRP) ratio increased from proximal (37.5±33.5) to distal (72.0±7.2 in the post-bifurcation segments; p<0.001). Thirty-eight neuroganglia were identified along 14 (78%) renal arteries.

Conclusions: Nerves converge to the renal arteries' lumen in the distal segments and along branches, resulting in the lowest number of nerves per quadrant and the shortest lumen-nerve distance in the distal post-bifurcation segments. Efferent nerves occur predominantly, and the ratio of efferent to afferent nerves continues to increase in the vessels' course.

**Corresponding author: Klinik für Innere Medizin III, Universitätsklinikum des Saarlandes and Saarland University, Kirrberger Straße 100, 66421 Homburg, Germany. Email: lucas.lauder@uks.eu*

SUBMITTED ON 00 - REVISION RECEIVED ON 1st 00 / 2nd 00 / 3rd 00 / 4th 00 - ACCEPTED ON 00

DOI: 10.4244/EIJ-D-23-00264

Abbreviations

CGRP	calcitonin gene-related peptide
H&E	haematoxylin and eosin
LND	lumen-nerve distance
RDN	renal denervation
SD	standard deviation
TH	tyrosine hydroxylase

Introduction

Renal denervation (RDN) was shown to lower blood pressure in several randomised sham-controlled trials[1-4] and represents an adjunct treatment option for patients with uncontrolled hypertension[5]. RDN modulates the activity of afferent and efferent sympathetic nerves in the perivascular tissue surrounding the renal arteries[6]. Both afferent and efferent sympathetic nerves are key players in blood pressure regulation. Mechanosensitive and chemosensitive afferent sympathetic nerves provide continuous feedback from the renal pelvic wall to the central nervous system. Efferent sympathetic renal nerve activity increases renin release, via β1-adrenergic receptor activation and renal tubular sodium reabsorption, and decreases renal blood flow[7]. The first-generation sham-controlled trial demonstrated safety but not the blood pressure-lowering efficacy of RDN compared with an invasive sham procedure and, thus, necessitated further investigation of the renal artery anatomy and renal innervation to improve technical performance as the peripheral branches were not treated in this trial[8]. A human autopsy study subsequently provided evidence that the lumen-nerve distance (LND) of periarterial renal sympathetic nerves is closest in distal vessel segments and dorsal locations. Data on nerve distribution in distal post-bifurcation segments come primarily from an autopsy study of 20 body donors (20% female, 35% African American), without characterisation of nerve type and function (e.g., afferent and efferent nerves)[9]. Further data are needed to refine the procedural technology and technique. A detailed understanding of renal nerve distribution and density may reduce the number of ablations, especially when using radiofrequency-based catheter systems, thereby decreasing the patient's and interventionalist's exposure to radiation, reducing the procedural duration and contrast use, and increasing patient comfort. This study aimed to assess renal nerve innervation in humans with a particular focus on the distal artery segments.

Methods

Ten body donors voluntarily consented to body donation during their lifetime at the Anatomical Institute of Saarland University, Homburg, Germany. The ethical committee of the Medical Association of Saarland approved the study (number 162/20).

PREPARATION OF HUMAN ARTERY TISSUE

The renal arteries were explanted within 24 hours after death to reduce the effect of autolysis[10]. After thoracotomy, the heart and lungs were removed, the abdomen was opened, and the gastrointestinal package was mobilised to reach the retroperitoneum with the renal arteries and the abdominal aorta. The liver, spleen, stomach, and kidneys were removed *en bloc*, including the renal arteries and the abdominal aorta. Both main renal arteries and any accessory renal arteries were dissected and extracted. Accessory renal arteries were defined as arteries other than the main renal artery[11]. The explantation of the vessels was performed carefully to prevent perivascular tissue and nerve damage.

All arteries were marked to ensure spatial orientation. After removal, all tissues of interest were stored in 4% formaldehyde (Otto Fischer GmbH) for 24 hours.

SECTIONING

After 24 hours in buffered 4% formaldehyde, the tissue was dissected into serial parts, 10 mm in length, and inserted into 1x1 cm embedding cassettes (Simport Scientific). Ascending alcohol series (HistoCore; Leica Biosystems) were used to dehydrate the tissue. Afterwards, the vessel and the surrounding tissue were embedded in paraffin (HistoCore Arcadia; Leica Biosystems), cut every 5 mm into 5 µm-thick slices using a microtome (HistoCore Autocut AS; Leica Biosystems) and mounted onto glass slides.

The division point in 2 or more consecutive branches of ≥3 mm diameter was defined as the end of the main renal artery. The renal arteries were classified into 3 segments of equal length: the proximal, middle, and distal segments. The distal vessel segments were termed prebifurcation or post-bifurcation, depending on whether the section was before or after the main artery bifurcation.

STAINING

Slides were stained with haematoxylin-eosin (H&E; Böhmer haematoxylin [Waldeck], eosin solution [Merck]) for an overview and to evaluate the slice quality. S100-staining (IR 504; Dako) was used to assess the distribution of neuronal tissue and nerves. To assess efferent sympathetic nerves, tyrosine hydroxylase (TH; anti-tyrosine hydroxylase: Abcam, ab112, sec.-ab: Anti-Rabbit FITC [Dianova, BIOZOL, 711-095-152]) staining was used **(Supplementary Figure 1)**. Afferent (sensory) nerves were stained with calcitonin gene-related peptide (CGRP; Anti-CGRP, Abcam, ab47027, sec.-ab: Anti-Rabbit FITC [Dianova, BIOZOL, 711-095-152]) **(Supplementary Figure 2)**.

HISTOLOGICAL ANALYSIS

Slides were scanned with a whole slide-scanner (Leica Aperio Versa 8; Leica Biosystems) at 10- to 20-fold magnification, and the histological analysis was performed with Leica Aperio ImageScope software (Leica Biosystems).

For each artery, one S100-stained slide was evaluated of the proximal segment, one of the middle segment, and for all existing sections in the distal segments **(Supplementary Figure 3)**. The arteries' lumina were divided into 4 quadrants based on markings, and assigned as ventral, superior, dorsal, and inferior areas.

The S100-stained sections were analysed for the amount, size, and LND of neuronal tissue in the perivascular area **(Figure 1)**. The LND was defined as the shortest distance from

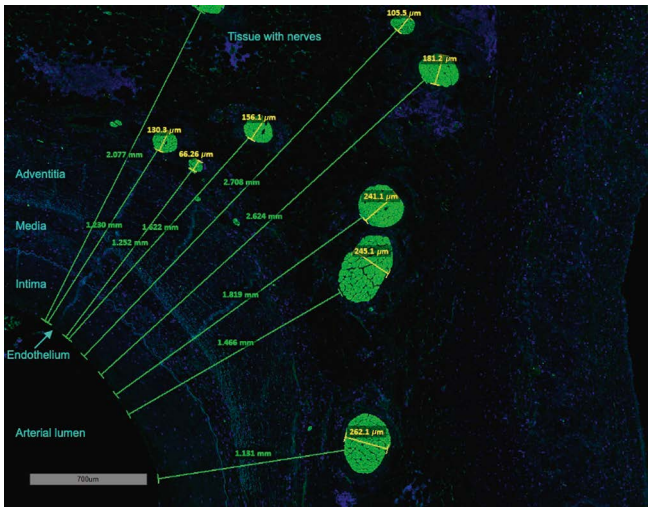

Figure 1. *Measurement of nerve size and lumen-nerve distance in S100-staining. The green lines and numbers represent the lumen-nerve distance from the endothelium to the proximal edge of the nerves (mm). Yellow lines and numbers indicate the smallest diameter of the nerves (µm).*

the inner endothelium to the edge of the nerve. These measurements were performed within a 10 mm radius from the endothelium. The nerves' sizes were classified, based on the smallest diameter, as small (35-69 µm), middle (70-140 µm), and large (>140 µm). Because of artefacts and inaccurate presentation, smaller nerves were not registered. Additionally, anatomical measurements of the vessel were performed, and the presence of lymph nodes, neuroganglia, and atherosclerotic change were documented.

Tissue slides were stained with TH according to the same scheme used for S100 staining. The number of nerves in each quadrant was determined, and the LND measured. Nerve density was related to each quadrant's total tissue area.

The ratio of efferent and afferent nerves was calculated by dividing the TH-positive area by the CGRP-positive area of the same nerves in the same section.

STATISTICAL ANALYSIS

All statistical analyses were performed using SPSS Statistics version 27.0 (IBM). Categorical variables were summarised as numbers (%), and continuous variables as mean±standard deviation (SD). Histograms and the Shapiro-Wilk test were used to assess normal distribution. Fisher's exact test and the Mann-Whitney U test were used for between-group comparisons of patients with and without a history of hypertension. Comparisons between arteries, segments, and regions were performed using the Kruskal-Wallis test. For comparisons between the left and the right renal arteries, the mean values per renal artery were calculated, and the Wilcoxon signed-rank test was used. A 2-tailed p-value<0.05 was considered statistically significant.

RESULTS

A total of 18 main renal arteries and 2 accessory renal arteries of 10 body donors were analysed. Of these, 2 body donors had a history of unilateral nephrectomy, and 3 had a history of chronic kidney disease.

The patient characteristics are summarised in **Table 1**. The mean lumen diameter of the renal arteries was 4.4±1.1 mm in the proximal, 3.6±1.4 mm in the middle and 3.8±2.4 mm in the distal segments (p=0.036).

NERVE DISTRIBUTION ALONG RENAL ARTERIES

A total of 94 slides (left artery n=47, right artery n=47) of the proximal (n=17), middle (n=15), distal prebifurcation (n=19), and post-bifurcation sections (n=43) of 18 renal arteries were analysed **(Table 2)**. These slides contained 3,506 nerves **(Table 3)**. The mean LND of nerves surrounding the left renal arteries was 2.32±1.95 mm and 2.29±2.03 mm for the right renal arteries (p=0.161). In the proximal, middle, distal prebifurcation, and distal post-bifurcation segments the LND was 3.7±2.3 mm (left renal arteries: 3.5±2.3; right renal arteries: 3.8±2.3; p=0.600 for comparison between left and right renal arteries), 2.5±2.0 mm (left: 2.2±1.7; right: 2.8±2.1; p=0.463), 1.9±1.6 mm (left: 2.2±1.7; right: 1.7±1.5; p=0.180), and 1.3±1.1 mm (left: 1.4±1.2; right: 1.2±1.0; p=0.075) (p<0.001 over all segments), respectively **(Table 4)**. The 50th, 75th, and 90th percentiles of the LND decreased from the proximal to the distal segments **(Figure 2)**. LND distribution according to regions is shown in **Figure 3**.

A total of 3,523 nerves were identified in S100-stained slides. The mean number of nerves per quadrant did not vary significantly between the left (6.3±8.7) and the right (7.6±9.7) renal arteries (p=0.889). However, it varied throughout the renal arteries'

Table 1. Body donors' characteristics.

Parameter	All body donors (n=10)	Non-hypertensive body donors (n=6)	Hypertensive body donors (n=4)	*p*-value*
Female	3 (30)	1 (17)	2 (50)	0.500
Age, years	84±8	87±5	79±9	0.257
Diabetes mellitus	5 (50)	3 (50)	2 (50)	1.000
Hyperlipidemia	3 (30)	2 (33)	1 (25)	1.000
Cardiovascular death	2 (20)	0 (0)	2 (50)	0.133
Data are summarised as mean±standard deviation or n (%). *p-values are calculated for comparisons between patients with and without hypertension.				

Table 2. Renal artery anatomy.

		All (n=10)*	Non-hypertensive (n=6)†	Hypertensive (n=4)‡	*p*-value§
External elastic area, mm²	left	17.3±18.4	20.4±22.6	12.3±4.5	0.572
	right	15.9±13.0	21.5±16.0	11.8±8.2	0.015
Internal elastic area, mm²	left	12.7±16.0	15.5±19.6	7.9±3.3	0.542
	right	11.6±11.4	16.4±14.4	8.1±6.8	0.021
Lumen area, mm²	left	9.0±11.9	11.4±14.5	5.0±2.6	0.413
	right	7.8±8.0	11.6±9.8	5.0±4.8	0.001
Lumen diameter, mm	left	3.8±2.4	4.3±2.8	3.0±0.8	0.180
	right	3.9±1.9	4.8±2.0	3.2±1.5	0.001
Media thickness, mm	left	0.3±0.1	0.3±0.1	0.3±0.2	0.326
	right	0.3±0.1	0.3±0.2	0.3±0.1	0.908
Renal arteries with atherosclerosis	left	3 (30)	2 (33)	1(25)	0.374
	right	4 (50)	2 (50)	2 (50)	1.000
Percentage of stenosis	left	28.0±11.8	19.0±6.5	38.0±6.7	0.008
	right	41.0±22.5	28.0±20.2	49.0±21.9	0.250
Renal arteries with lymph nodes	left	7 (70)	4 (67)	3 (75)	0.374
	right	6 (75)	4 (100)	2 (50)	0.472
Renal arteries with neuroganglia	left	7 (70)	5 (83)	2 (50)	1.000
	right	7 (88)	4 (100)	3 (75)	0.510

Data are summarised as means±standard deviation or n (%). *10 left renal arteries and 8 right renal arteries. †6 left renal arteries and 4 right renal arteries. ‡4 left renal arteries and 4 right renal arteries. §p-values were calculated for comparisons between patients with and without hypertension.

Table 3. Number of nerves according to lumen-nerve distance.

Lumen-nerve distance	Number of nerves				
	Proximal segment	Middle segment	Distal prebifurcation segment	Distal post-bifurcation segment	Total
0-1 mm	77	142	177	615	1,011
1-2 mm	202	325	235	420	1,182
2-3 mm	143	117	72	79	411
3-4 mm	124	79	29	33	265
4-5 mm	140	71	27	24	262
5-6 mm	83	32	14	5	134
6-7 mm	57	29	7	2	95
7-8 mm	34	9	8	6	57
8-9 mm	39	6	4	0	49
9-10 mm	19	16	3	2	40
Total	918	826	576	1,186	3,506

Data are counts.

courses and was highest in the proximal (13.7±18.6 nerves per quadrant) versus the middle (9.7±7.9) and the distal prebifurcation segments (8.0±7.6) and was lowest in distal post-bifurcation segments (4.3±4.0; p<0.001). Overall, the highest numbers of nerves per quadrant were identified in the superior (7.8±9.4) and ventral (7.6±3.1) quadrants **(Table 4)**.

Two accessory renal arteries with a mean lumen diameter of 2.2±0.9 mm were identified. A total of 71 nerves surrounding these accessory renal arteries were analysed. The mean LND of these nerves was 2.6±2.2 mm.

We identified 38 neuroganglia along 14 (78%) renal arteries. Neuroganglia were found most frequently in the proximal artery segments (proximal segment 47.4%, middle segment 34.2%, distal prebifurcation segment 15.8%, and distal post-bifurcation segment 2.6%) and the ventral region (31.6%) **(Supplementary Table 1)**. Thirteen of 18 renal arteries had lymph nodes within a 10 mm radius.

NERVE NUMBER DENSITY PER ANALYSED AREA

The mean nerve number density, calculated as the number of nerves per tissue area, was 66.3 nerves per cm² (53.5 nerves per cm² for the

Table 4. Lumen-nerve distance according to renal artery segments and regions.

Region	Segment									
	Proximal segment		Middle segment		Distal prebifurcation segment		Distal post-bifurcation segment		Overall	
	Mean±SD	N	Mean±SD	N	Mean±SD	N	Mean±SD	N	Mean±SD	N
Number of nerves per quadrant										
Ventral	20.4±30.1	18	9.5±7.6	20	6.8±4.9	18	3.8±3.6	73	7.5±13.1	129
Superior	16.7±15.5	18	11.8±9.3	20	10.2±9.5	18	3.8±3.2	70	7.8±9.4	126
Dorsal	9.3±8.2	17	10.3±7.4	21	7.2±7.5	18	4.5±4.2	69	6.5±6.4	125
Inferior	7.4±8.3	16	7.3±7.3	21	7.7±7.7	20	5.0±4.8	69	6.1±6.3	126
Overall	13.7±18.6	69	9.7±7.9	82	8.0±7.6	74	4.3±4.0	281	7.0±9.3	506
Lumen-nerve distance, mm										
Ventral	4.2±2.4	362	3.0±2.2	195	1.8±1.4	116	1.2±0.8	271	2.8±2.3	944
Superior	3.8±2.3	283	2.8±2.2	251	2.1±1.8	183	1.3±1.2	262	2.6±2.2	979
Dorsal	2.6±1.9	154	2.2±1.4	221	1.3±0.8	130	1.3±1.0	307	1.8±1.4	812
Inferior	2.9±1.9	119	2.1±1.6	159	2.2±1.9	147	1.4±1.2	346	1.9±1.7	771
Overall	3.7±2.3	918	2.5±2.0	826	1.9±1.6	576	1.3±1.1	1,186	2.3±2.0	3,506
Data are summarised as means±standard deviation (SD).										

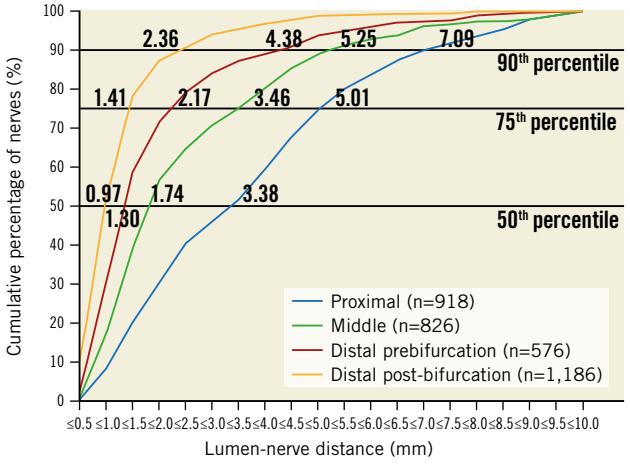

Figure 2. *Renal nerve distribution according to lumen-nerve distance. Cumulative percentage of the lumen-nerve distance (LND) in different segments. Numbers indicate the LND at the 90th, 75th, and 50th percentiles for nerves in the proximal, middle, distal prebifurcation, and distal post-bifurcation segments.*

left and 78.7 nerves per cm² for the right renal arteries; p=0.161). It was highest in the distal post-bifurcation segments (70.9 nerves per cm²), followed by the middle (66.3 nerves per cm²), the distal prebifurcation (60.2 nerves per cm²), and the proximal segments (54.0 nerves per cm²) (p=0.001 global). Regarding circumferential distribution, the nerve density did not differ statistically significantly between the ventral (76.5 nerves per cm²), superior (63.5 nerves per cm²), inferior (65.3 nerves per cm²), or dorsal quadrants (59.6 nerves per cm²; p=0.669).

SIZE OF NERVES

In all vessel segments, most nerves were small **(Supplementary Table 2)**. The proportion of small nerves (diameter 35-69 µm) increased from proximal to distal (proximal 43%, middle 48%, and distal 54%), whereas the proportion of middle-sized (diameter 70-139 µm) and large (diameter ≥140 µm) nerves decreased.

ANALYSIS OF EFFERENT NERVES IN RENAL ARTERIES

A total of 2,864 nerves were measured for LND with TH-staining. The mean LND of nerves surrounding the left (n=1392) and right (n=1472) renal arteries were 2.09±1.78 mm and 2.08±1.75 mm, respectively (p=0.779). In proximal (15 slides), middle (17 slides), distal prebifurcation (20 slides), and distal post-bifurcation (43 slides) segments, the mean LND was 3.2±2.1 mm, 2.6±1.8 mm, 1.7±1.3 mm, and 1.2±1.0 mm, respectively (p<0.001). The LND of nerves differed significantly between the inferior (1.9±1.6 mm) and superior (2.4±2.2 mm) quadrants (p=0.014) and between the dorsal (1.9±1.4 mm) and superior quadrants (p=0.015). There was no significant difference between the other quadrants (p>0.05). The ventral quadrant had a mean LND of 2.1±1.6 mm.

ANALYSIS OF THE RATIO OF EFFERENT AND AFFERENT NERVES

The proportion of efferent (sympathetic) and afferent (sensory) nerves were examined in 5 representative renal arteries of 4 patients with 411 nerves in 19 sections (5 sections in the proximal, 5 in the middle, 4 in the distal prebifurcation, and 5 in the distal post-bifurcation segments). The overall TH-positive area (95.5±5.9%) was significantly larger than the CGRP-positive area (4.5±5.9%). The mean TH/CGRP ratio, calculated as the ratio of the TH-positive to CGRP-positive area, of surrounding nerves within 10 mm distance from the endothelium did not differ between the left (52.8±48.5) and right renal arteries (56.1±46.4; p=0.109). The TH/CGRP ratio increased along the renal arteries' courses. In the proximal, middle, distal prebifurcation, and distal post-bifurcation segments, the TH/

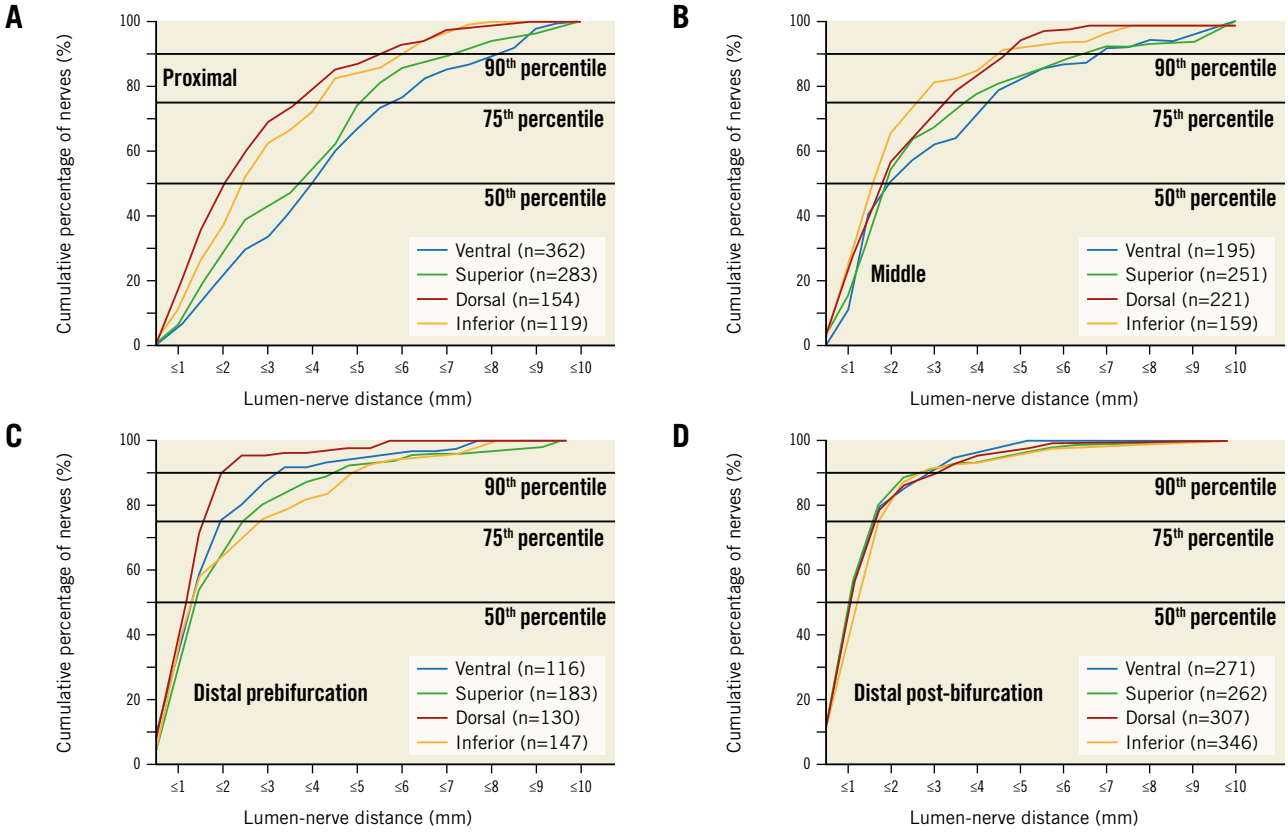

Figure 3. *Cumulative percentile of lumen-nerve distance according to regions. The graphs represent different regions in the proximal (A), middle (B), distal prebifurcation (C), and distal post-bifurcation (D) segments.*

CGRP ratio was 37.5±33.5, 56.0±48.3, 70.2±46.0, and 72.0±57.2, respectively (p<0.001). There was a significant difference between the proximal and the middle and distal segments (proximal vs middle: p=0.003; proximal vs distal segments: p<0.001), but not between the middle, distal prebifurcation, and distal post-bifurcation segments (all p>0.05). The percentage distribution of segments is shown in **Supplementary Table 3**.

Discussion

This study assessed the nerve distribution along renal arteries of human body donors, focusing on the post-bifurcation vessel segments. In line with previous studies[9], nerves converge to the renal arteries' lumen in the distal segments and along the branches, resulting in the shortest LND in the distal post-bifurcation segments. Efferent nerves occur predominantly, and the ratio of efferent to afferent nerves continues to increase along the vessels' course **(Central illustration)**. The current study extends previous studies, as it is the first to show that the nerve density and the ratio of efferent and afferent nerves (TH/CGRP ratio) increase from proximal to distal and are numerically highest in the post-bifurcation segments. Moreover, 90% of nerves are located within 5.11 mm from the lumen. These findings facilitate the optimisation of RDN technology and techniques.

While the number of nerves per quadrant was highest in proximal renal artery segments and decreased along the course of the vessel, in line with previous human cadaver studies, the mean LND was found to be lowest in the distal segments, particularly post-bifurcation[9,12]. When looking at the entire vessel, 90% of the nerves are located within 5.11 mm from the lumen. Thus, the nerves are considerably closer to the renal arteries in this study than in previous studies[9,13]. One may argue that this is related to the identification of smaller nerves (82% of nerves were <140 µm in this study vs 73% of nerves <150 µm in previous studies)[9] by using a higher magnification than previous studies (10-20x magnification compared with 1.25x magnification[9,13]). Moreover, the distribution could also slightly differ across populations and geographies.

While in proximal segments, 90% of the nerves are located within 7.1 mm distance from the renal artery, in distal post-bifurcation segments, 90% are located within 2.4 mm. For radiofrequency RDN devices, the mean lesion depth is approximately 3.8 mm[14]. According to the nerve distribution in this study, a catheter with a penetration depth of 3.8 mm would affect more than 90% of the nerves in the distal post-bifurcation segments and 75-90% of the nerves in the middle and distal prebifurcation segments but only 50-60% in the proximal segments. In contrast to the number of nerves per quadrant, which decreased from proximal to distal, there was a trend towards a higher nerve density in the distal post-bifurcation segments than the more proximal artery segments. The amount of extracted perivascular tissue decreased along the renal arteries. At the same time, the nerve density increased, indicating that the number of potentially

CENTRAL ILLUSTRATION Distribution of nerves in segments of renal arteries.

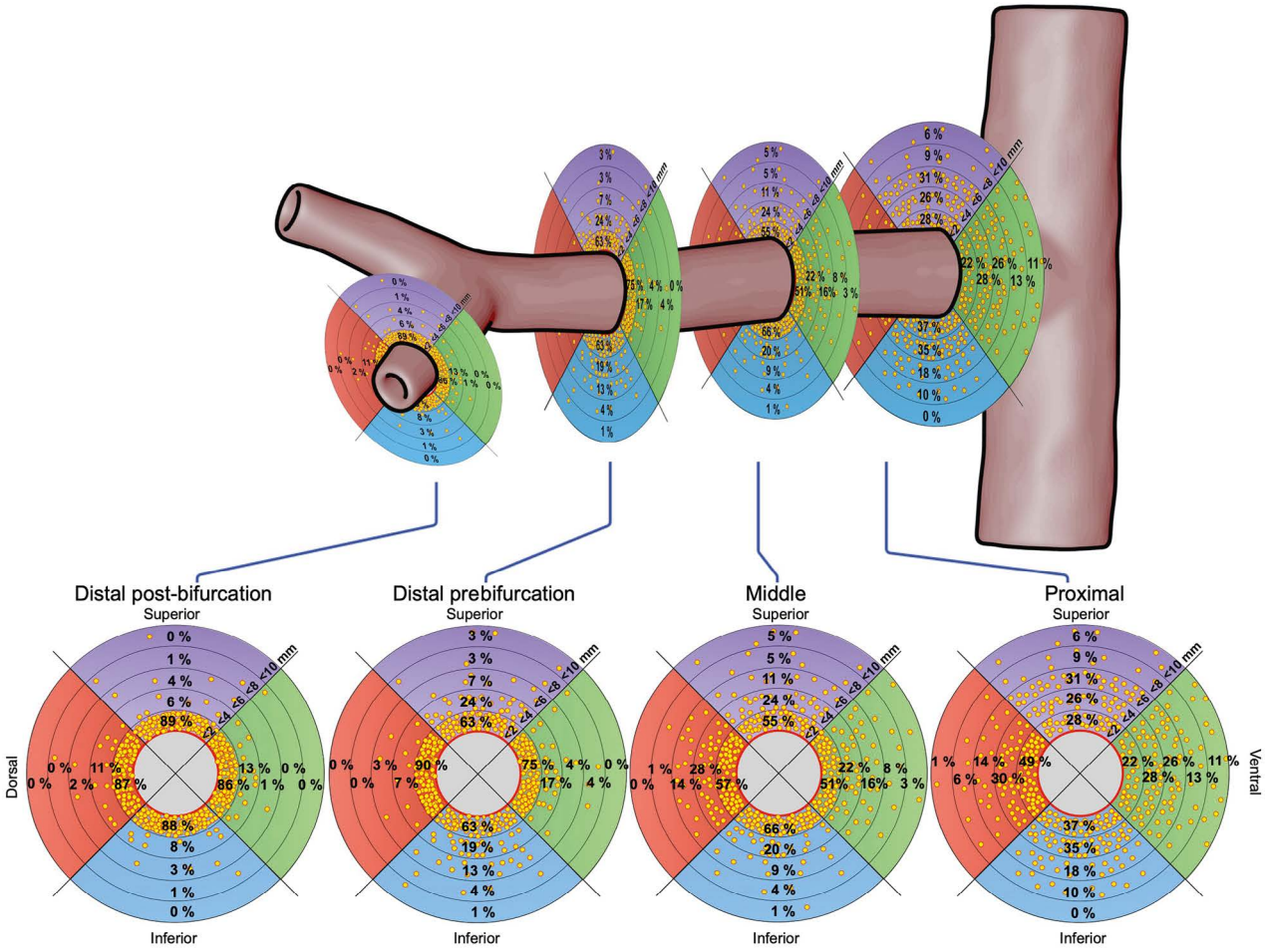

The plots show the percentage of nerves in regions within <2, <4, <6, <8, and <10 mm from the renal arteries' lumen.

treatable nerves increased in the distal vascular segments. Data on nerve distribution in post-bifurcation segments are scarce, although radiofrequency catheters allow for the treatment of vessels, including branches, outside the renal parenchyma ranging in diameter between 3 and 8 mm. In line with this, preclinical and clinical studies encourage the treatment of branches and distal artery segments in addition to the main renal artery when performing radiofrequency RDN[15]. In a porcine model, treatment of branches in addition to the main renal arteries using radiofrequency RDN resulted in the least variability of response and a significantly greater reduction in norepinephrine and axon density than treatment of the main renal artery only[16]. In clinical studies, the same ablation strategy resulted in more pronounced and reproducible blood pressure reductions[15,17]. It is desirable to reduce the number of ineffective ablation attempts to make the procedure more cost-effective and safer by reducing procedural time, contrast agent use, and radiation dose. In the SPYRAL HTN-OFF MED Pivotal trial, for example, the mean procedure time was 100 minutes for a mean of 46.9 total ablations[2]. For catheter systems with less penetration depth, treatment of distal segments and branches might affect higher numbers of renal nerves and be more efficient than treatment of proximal segments. Importantly, ablations should only be performed in segments outside the renal parenchyma, as observed on fluoroscopy, to avoid potential parenchymal kidney damage. Computational analyses have shown that the low conductivity of adipose tissue, in which most renal nerves are embedded, results in a greater resistive loss and heating of fat tissue than other perivascular tissue. Reassuringly, in a porcine model, treatment of the branches resulted in only minimal perivascular tissue damage[12]. In sham-controlled RDN trials with radiofrequency ablations in the branches, there was no signal of impaired kidney function at 3 years after RDN [5].

Previous studies reported conflicting results regarding the circumferential distribution of nerves[9,13,18,19]. This study identified the most nerves per quadrant in the superior and ventral quadrants. Looking only at the post-bifurcation segment, the number of nerves per quadrant was highest in the dorsal and inferior quadrants. Moreover, previous studies usually calculated renal nerve

distribution as the number of nerves per artery or segment[9,13]. As the area of periarterial tissue varies across segments and quadrants, we calculated the nerve density, defined as the number of nerves per area of periarterial tissue.

About 95% of the stained area contained efferent (TH-positive) nerves[9,20]. This is particularly important, as stimulation of efferent nerves causes renin release via β1-adrenergic receptor activation at the level of the juxtaglomerular cells[21], increases renal tubular sodium reabsorption via alpha1-adrenoceptors[22], and decreases renal blood flow by causing alpha-adrenoceptor-mediated renal vasoconstriction[23]. The relative increase of efferent nerves from proximal to distal might partially explain why a reduction in heart rate and plasma renin activity was observed following radiofrequency RDN of the main renal arteries and their branches[24,25] but not for ultrasound RDN of the main renal arteries only[24,26]. Knowledge of the distribution of efferent and afferent nerves is essential for developing new devices and using existing devices in novel indications if primarily afferent or efferent nerves are to be targeted.

In addition, surrounding lymph nodes and atherosclerotic plaques should be considered when targeting the renal nerves, as these can act as heat sinks[27]. Lymph nodes are usually not damaged by RDN, as higher electrical conductivity and convective heat conduction from flowing fluid inhibit temperature increases in these tissues[12]. However, surrounding lymph nodes affect the uniformity and circumferential spread of thermal energy that most catheter systems use for ablation. Moreover, 39% of the renal arteries were affected by atherosclerotic changes resulting in lumen narrowing. These atherosclerotic changes might also limit the efficacy of RDN by increasing the lumen-nerve distance[28]. Neuroganglia were present along most renal arteries. The impact of ablating non-specific neuroganglia potentially carrying innervation to the kidneys and potentially to other abdominal and pelvic organs[12] is uncertain. In line with previous studies, most neuroganglia were in the proximal and middle renal artery segments[12]. By focusing on the distal renal artery segments, non-specific neuroganglia are less likely to be affected by the ablation lesions.

Limitations

Some limitations of this anatomy study must be acknowledged. First, although we analysed almost 7,000 nerves, this study included 10, predominantly male (70%), elderly Caucasian body donors from Germany. Therefore, the results of this study may not fully be translatable to other populations or geographies. Second, the study size is too small to perform subgroup analyses. As only 2 accessory arteries were found, we did not perform comparisons between the main and accessory renal arteries. Third, tissue shrinkage usually occurs when using formalin fixation[9]. Moreover, no perfusion fixation was used, which, in part, limits the comparability of exact distances, such as LND, across studies. Importantly, observations on nerve distribution and function throughout the vessels course within this study are most likely not affected. We did not adjust for tissue shrinkage due to age dependency and *ex vivo* assessment.

Conclusions

Nerves converge to the lumen of the renal artery in the distal segments and along the branches, resulting in the lowest number of nerves per quadrant and the shortest LND in the distal post-bifurcation segments. As the ratio of efferent to afferent nerves increases in the vessels' course, the post-bifurcation segment may represent an attractive treatment area if efferent nerve signalling is targeted. These findings will help to optimise the procedural performance of RDN and catheter development.

Impact on daily practice

This histological examination of cadaveric human renal arteries demonstrates that nerves converge to the renal arteries' lumen in the distal segments and along branches, resulting in the lowest number of nerves per quadrant and the shortest lumen-nerve distance in the distal post-bifurcation segments. Efferent nerves occur predominantly, and the ratio of efferent to afferent nerves continues to increase in the vessels' course. These insights into renal nerve distribution will guide renal denervation, as they suggest that the number of potentially treatable nerves increases in the distal artery segments.

Acknowledgements

We sincerely thank those who donated their bodies to science for anatomical research. Results from such research can potentially increase humankind's overall knowledge, which can then improve patient care. Therefore, these donors and their families deserve our highest gratitude.

We gratefully acknowledge Julia Weber and Jeannette Zimolong for their excellent technical support and Armin Schweitzer for helping us with the artwork.

Conflict of interest statement

L. Lauder received speaker honoraria from ReCor Medical and Medtronic. M. Böhm is supported by the Deutsche Forschungsgemeinschaft (German Research Foundation; SFB-TTR 219, project number 322900939) and reports personal fees from Abbott, Amgen, AstraZeneca, Bayer, Boehringer Ingelheim, Cytokinetics, Edwards Lifesciences, Medtronic, Novartis, ReCor Medical, Servier, and Vifor during the conduct of the study. F. Mahfoud is supported by Deutsche Gesellschaft für Kardiologie (DGK), Deutsche Forschungsgemeinschaft (German Research Foundation; SFB-TTR 219, project number 322900939), and Deutsche Herzstiftung. He has received scientific support from Ablative Solutions, Medtronic, and ReCor Medical; and speaker honoraria/consulting fees from Ablative Solutions, Amgen, AstraZeneca, Bayer, Boehringer Ingelheim, Inari, Medtronic, Merck, ReCor Medical, Servier, and Terumo. E.R. Edelman was funded, in part, by a grant (R01 HL 161069) from the US National Institutes of Health. The other authors report no conflicts of interest.

References

1. Azizi M, Sanghvi K, Saxena M, Gosse P, Reilly JP, Levy T, Rump LC, Persu A, Basile J, Bloch MJ, Daemen J, Lobo MD, Mahfoud F, Schmieder RE, Sharp ASP, Weber MA, Sapoval M, Fong P, Pathak A, Lantelme P, Hsi D, Bangalore S, Witkowski A, Weil J, Kably B, Barman NC, Reeve-Stoffer H, Coleman L, McClure CK, Kirtane AJ; RADIANCE-HTN investigators. Ultrasound renal denervation for hypertension resistant to a triple medication pill (RADIANCE-HTN TRIO): a randomised, multicentre, single-blind, sham-controlled trial. *Lancet.* 2021;397:2476-86.

2. Böhm M, Kario K, Kandzari DE, Mahfoud F, Weber MA, Schmieder RE, Tsioufis K, Pocock S, Konstantinidis D, Choi JW, East C, Lee DP, Ma A, Ewen S, Cohen DL, Wilensky R, Devireddy CM, Lea J, Schmid A, Weil J, Agdirlioglu T, Reedus D, Jefferson BK, Reyes D, D'Souza R, Sharp ASP, Sharif F, Fahy M, DeBruin V, Cohen SA, Brar S, Townsend RR; SPYRAL HTN-OFF MED Pivotal Investigators. Efficacy of catheter-based renal denervation in the absence of antihypertensive medications (SPYRAL HTN-OFF MED Pivotal): a multicentre, randomised, sham-controlled trial. *Lancet.* 2020;395:1444-51.

3. Kandzari DE, Böhm M, Mahfoud F, Townsend RR, Weber MA, Pocock S, Tsioufis K, Tousoulis D, Choi JW, East C, Brar S, Cohen SA, Fahy M, Pilcher G, Kario K; SPYRAL HTN-ON MED Trial Investigators. Effect of renal denervation on blood pressure in the presence of antihypertensive drugs: 6-month efficacy and safety results from the SPYRAL HTN-ON MED proof-of-concept randomised trial. *Lancet.* 2018;391:2346-55.

4. Azizi M, Schmieder RE, Mahfoud F, Weber MA, Daemen J, Davies J, Basile J, Kirtane AJ, Wang Y, Lobo MD, Saxena M, Feyz L, Rader F, Lurz P, Sayer J, Sapoval M, Levy T, Sanghvi K, Abraham J, Sharp ASP, Fisher NDL, Bloch MJ, Reeve-Stoffer H, Coleman L, Mullin C, Mauri L; RADIANCE-HTN Investigators. Endovascular ultrasound renal denervation to treat hypertension (RADIANCE-HTN SOLO): a multicentre, international, single-blind, randomised, sham-controlled trial. *Lancet.* 2018;391:2335-45.

5. Barbato E, Azizi M, Schmieder RE, Lauder L, Böhm M, Brouwers S, Bruno RM, Dudek D, Kahan T, Kandzari DE, Lüscher TF, Parati G, Pathak A, Ribichini FL, Schlaich MP, Sharp ASP, Sudano I, Volpe M, Tsioufis C, Wijns W, Mahfoud F. Renal denervation in the management of hypertension in adults. A clinical consensus statement of the ESC Council on Hypertension and the European Association of Percutaneous Cardiovascular Interventions (EAPCI). *EuroIntervention.* 2023;18:1227-43.

6. Lauder L, Azizi M, Kirtane AJ, Böhm M, Mahfoud F. Device-based therapies for arterial hypertension. *Nat Rev Cardiol.* 2020;17:614-28.

7. DiBona GF, Esler M. Translational medicine: the antihypertensive effect of renal denervation. *Am J Physiol Regul Integr Comp Physiol.* 2010;298:R245-53.

8. Kandzari DE, Bhatt DL, Brar S, Devireddy CM, Esler M, Fahy M, Flack JM, Katzen BT, Lea J, Lee DP, Leon MB, Ma A, Massaro J, Mauri L, Oparil S, O'Neill WW, Patel MR, Rocha-Singh K, Sobotka PA, Svetkey L, Townsend RR, Bakris GL. Predictors of blood pressure response in the SYMPLICITY HTN-3 trial. *Eur Heart J.* 2015;36:219-27.

9. Sakakura K, Ladich E, Cheng Q, Otsuka F, Yahagi K, Fowler DR, Kolodgie FD, Virmani R, Joner M. Anatomic assessment of sympathetic peri-arterial renal nerves in man. *J Am Coll Cardiol.* 2014;64:635-43.

10. Maleszewski J, Lu J, Fox-Talbot K, Halushka MK. Robust immunohistochemical staining of several classes of proteins in tissues subjected to autolysis. *J Histochem Cytochem.* 2007;55:597-606.

11. Lauder L, Ewen S, Tzafriri A, Edelman ER, Lüscher T, Blankestijn P, Dörr O, Schlaich MP, Sharif F, Voskuil M, Zeller T, Ukena C, Scheller B, Böhm M, Mahfoud F; Renal artery anatomy in hypertensive patients study collaborators. Renal artery anatomy assessed by quantitative analysis of selective renal angiography in 1,000 patients with hypertension. *EuroIntervention.* 2018;14:121-8.

12. Sato Y, Sharp ASP, Mahfoud F, Tunev S, Forster A, Ellis M, Gomez A, Dhingra R, Ullman J, Schlaich M, Lee D, Trudel J, Hettrick DA, Kandzari DE, Virmani R, Finn AV. Translational value of preclinical models for renal denervation: a histological comparison of human versus porcine renal nerve anatomy. *EuroIntervention.* 2023;18:e1120-8.

13. Sato Y, Kawakami R, Jinnouchi H, Sakamoto A, Cornelissen A, Mori M, Kawai K, Guo L, Coleman L, Nash S, Claude L, Barman NC, Romero M, Kolodgie FD, Virmani R, Finn AV. Comprehensive Assessment of Human Accessory Renal Artery Periarterial Renal Sympathetic Nerve Distribution. *JACC Cardiovasc Interv.* 2021;14:304-15.

14. Al Raisi SI, Pouliopoulos J, Barry MT, Swinnen J, Thiagalingam A, Thomas SP, Sivagangabalan G, Chow C, Chong J, Kizana E, Kovoor P. Evaluation of lesion and thermodynamic characteristics of Symplicity and EnligHTN renal denervation systems in a phantom renal artery model. *EuroIntervention.* 2014;10:277-84.

15. Fengler K, Ewen S, Höllriegel R, Rommel KP, Kulenthiran S, Lauder L, Cremers B, Schuler G, Linke A, Böhm M, Mahfoud F, Lurz P. Blood Pressure Response to Main Renal Artery and Combined Main Renal Artery Plus Branch Renal Denervation in Patients With Resistant Hypertension. *J Am Heart Assoc.* 2017;6:e006196.

16. Mahfoud F, Tunev S, Ewen S, Cremers B, Ruwart J, Schulz-Jander D, Linz D, Davies J, Kandzari DE, Whitbourn R, Böhm M, Melder RJ. Impact of Lesion Placement on Efficacy and Safety of Catheter-Based Radiofrequency Renal Denervation. *J Am Coll Cardiol.* 2015;66:1766-75.

17. Fengler K, Rommel KP, Blazek S, Besler C, Hartung P, von Roeder M, Petzold M, Winkler S, Höllriegel R, Desch S, Thiele H, Lurz P. A Three-Arm Randomized Trial of Different Renal Denervation Devices and Techniques in Patients With Resistant Hypertension (RADIOSOUND-HTN). *Circulation.* 2019;139:590-600.

18. Mompeo B, Maranillo E, Garcia-Touchard A, Larkin T, Sanudo J. The gross anatomy of the renal sympathetic nerves revisited. *Clin Anat.* 2016;29:660-4.

19. Imnadze G, Balzer S, Meyer B, Neumann J, Krech RH, Thale J, Franz N, Warnecke H, Awad K, Hayek SS, Devireddy C. Anatomic Patterns of Renal Arterial Sympathetic Innervation: New Aspects for Renal Denervation. *J Interv Cardiol.* 2016;29:594-600.

20. Tellez A, Rousselle S, Palmieri T, Rate WR 4th, Wicks J, Degrange A, Hyon CM, Gongora CA, Hart R, Grundy W, Kaluza GL, Granada JF. Renal artery nerve distribution and density in the porcine model: biologic implications for the development of radiofrequency ablation therapies. *Transl Res.* 2013;162:381-9.

21. Osborn JL, DiBona GF, Thames MD. Beta-1 receptor mediation of renin secretion elicited by low-frequency renal nerve stimulation. *J Pharmacol Exp Ther.* 1981;216:265-9.

22. Dibona GF, Kopp UC. Neural control of renal function. *Physiol Rev.* 1997;77:75-197.

23. Kopp U, Aurell M, Sjölander M, Ablad B. The role of prostaglandins in the alpha- and beta-adrenoceptor mediated renin release response to graded renal nerve stimulation. *Pflugers Arch.* 1981; 391:1-8.

24. Gosse P, Cremer A, Kirtane AJ, Lobo MD, Saxena M, Daemen J, Wang Y, Stegbauer J, Weber MA, Abraham J, Kario K, Bangalore S, Claude L, Liu Y, Azizi M. Ambulatory Blood Pressure Monitoring to Predict Response to Renal Denervation: A Post Hoc Analysis of the RADIANCE-HTN SOLO Study. *Hypertension.* 2021;77:529-36.

25. Mahfoud F, Townsend RR, Kandzari DE, Kario K, Schmieder RE, Tsioufis K, Pocock S, David S, Patel K, Rao A, Walton A, Bloom JE, Weber T, Suppan M, Lauder L, Cohen SA, McKenna P, Fahy M, Böhm M, Weber MA. Changes in Plasma Renin Activity After Renal Artery Sympathetic Denervation. *J Am Coll Cardiol.* 2021;77:2909-19.

26. Fisher NDL, Kirtane AJ, Daemen J, Rader F, Lobo MD, Saxena M, Abraham J, Schmieder RE, Sharp ASP, Gosse P, Claude L, Song Y, Azizi M; RADIANCE-HTN Investigators. Plasma renin and aldosterone concentrations related to endovascular ultrasound renal denervation in the RADIANCE-HTN SOLO trial. *J Hypertens.* 2022;40:221-8.

27. Tzafriri AR, Keating JH, Markham PM, Spognardi AM, Stanley JRL, Wong G, Zani BG, Highsmith D, O'Fallon P, Fuimaono K, Mahfoud F, Edelman ER. Arterial microanatomy determines the success of energy-based renal denervation in controlling hypertension. *Sci Transl Med.* 2015;7:285ra65.

28. Vink EE, Goldschmeding R, Vink A, Weggemans C, Bleijs RL, Blankestijn PJ. Limited destruction of renal nerves after catheter-based renal denervation: results of a human case study. *Nephrol Dial Transplant.* 2014;29:1608-10.

Supplementary data

Supplementary Table 1. Distribution of neuroganglia.

Supplementary Table 2. Nerve fascicle size.

Supplementary Table 3. Distribution of TH/CGRP area in segments.

Supplementary Figure 1. Representative image of TH-staining in the proximal segment of the left renal artery.

Supplementary Figure 2. Representative image of a CGRP-stained nerve.

Supplementary Figure 3. Representative images of haematoxylin and eosin (H&E)- and S100-stained slides of different renal artery segments.

The supplementary data are published online at: https://eurointervention.pcronline.com/doi/10.4244/EIJ-D-23-00264

Supplementary data

Supplementary Table 1. Distribution of neuroganglia.

Segment	Number of neuroganglia				
	Ventral quadrant	**Superior quadrant**	**Dorsal quadrant**	**Inferior quadrant**	**Overall**
Proximal	6	4	3	5	18
Middle	6	3	3	1	13
Distal pre-bifurcation	0	2	0	4	6
Distal post-bifurcation	0	0	0	1	1
Total	12	9	6	11	38

Data are summarised as counts n.

Supplementary Table 2. Nerve fascicle size.

Nerve fascicle diameter	**Proximal segment n (%)**	**Middle segment n (%)**	**Distal segment n (%)**	**Overall n (%)**
Small (35-69 μm)	396 (43)	399 (48)	957 (54)	1752 (50)
Medium (70-139 μm)	324 (35)	274 (33)	522 (30)	1120 (32)
Large (≥140 μm)	198 (22)	153 (19)	283 (16)	634 (18)

Data are summarised as counts n (%).

Supplementary Table 3. Distribution of TH/CGRP area in segments.

Positive stained area	**Proximal segment, mean±SD**	**Middle segment, mean±SD**	**Distal pre-bifurcation segment, mean±SD**	**Distal post-bifurcation segment, mean %±SD**	**Overall, mean±SD**
TH-positive, %	94.2±7.3	96.1±4.4	95.9±7.0	96.6±4.5	95.5±5.9
CGRP-positive, %	5.8±7.3	3.9±4.4	4.1±7.0	3.4±4.5	4.5±5.9

Data are summarised as mean % ± standard deviation.

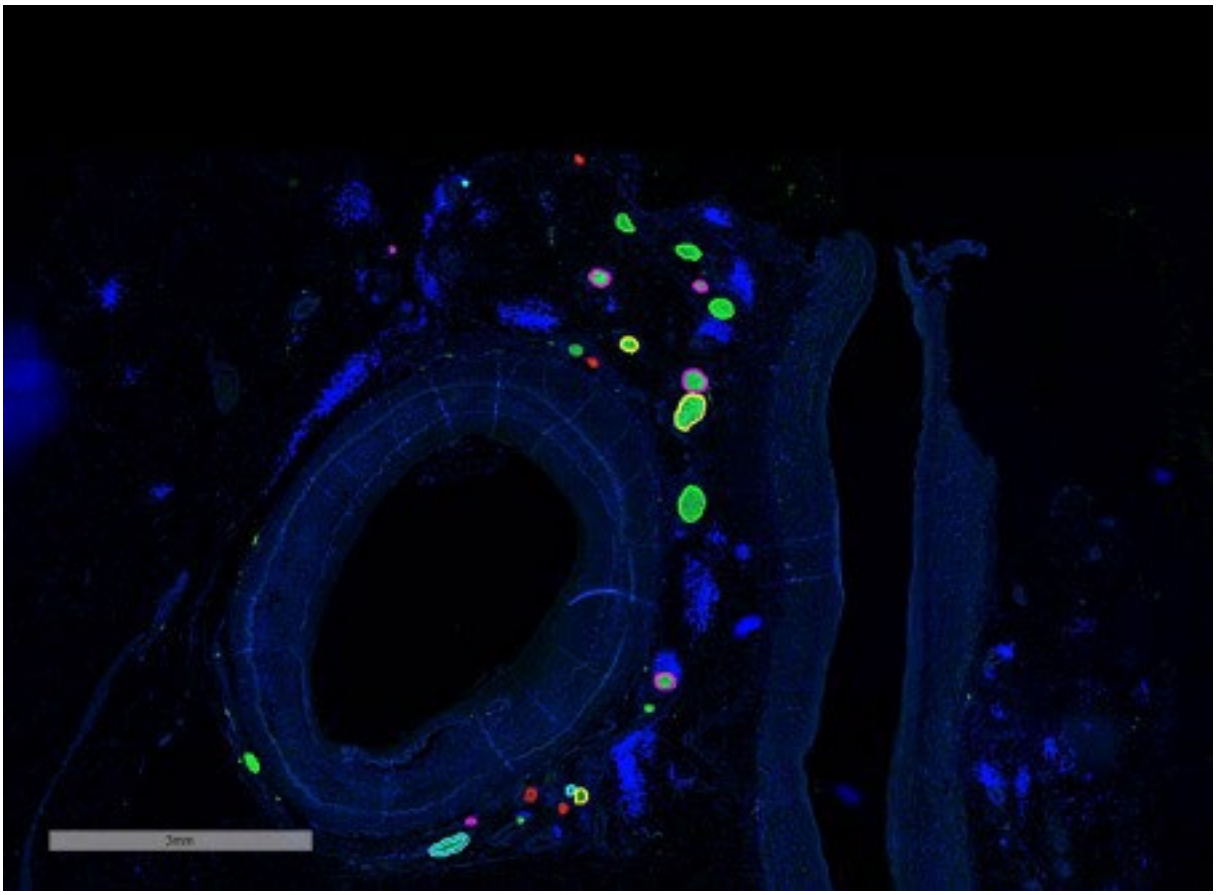

Supplementary Figure 1. Representative image of TH-staining in the proximal segment of the left renal artery.

Green channel: tyrosine-hydroxylase (TH)-positive nerves. Colored markers surround nerves. The scale bar represents 3 mm.

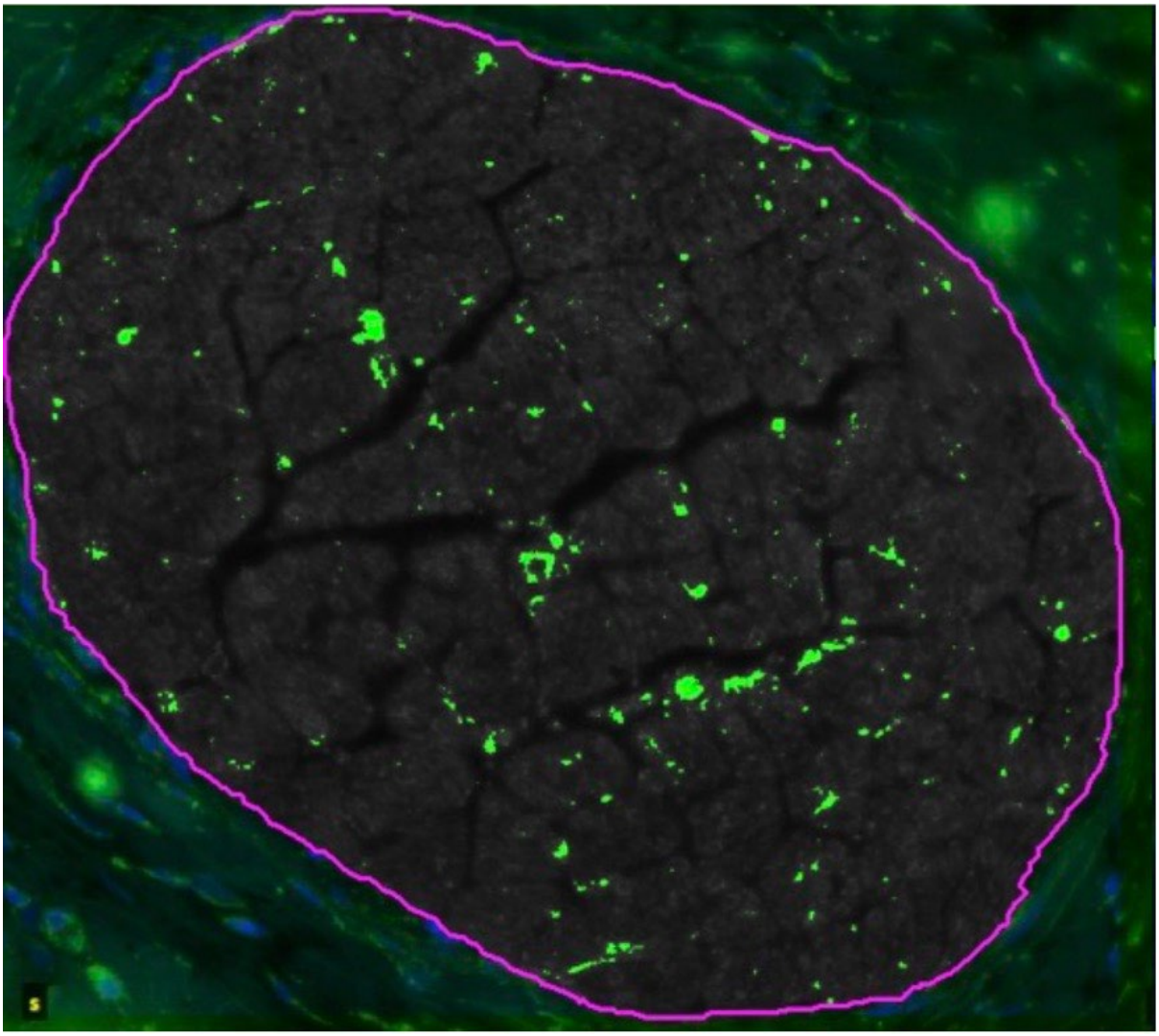

Supplementary Figure 2. Representative image of a CGRP-stained nerve.

The magenta-colored line indicates the outside boundary of the nerve. Green-channel: CGRP-positive area of the nerve.

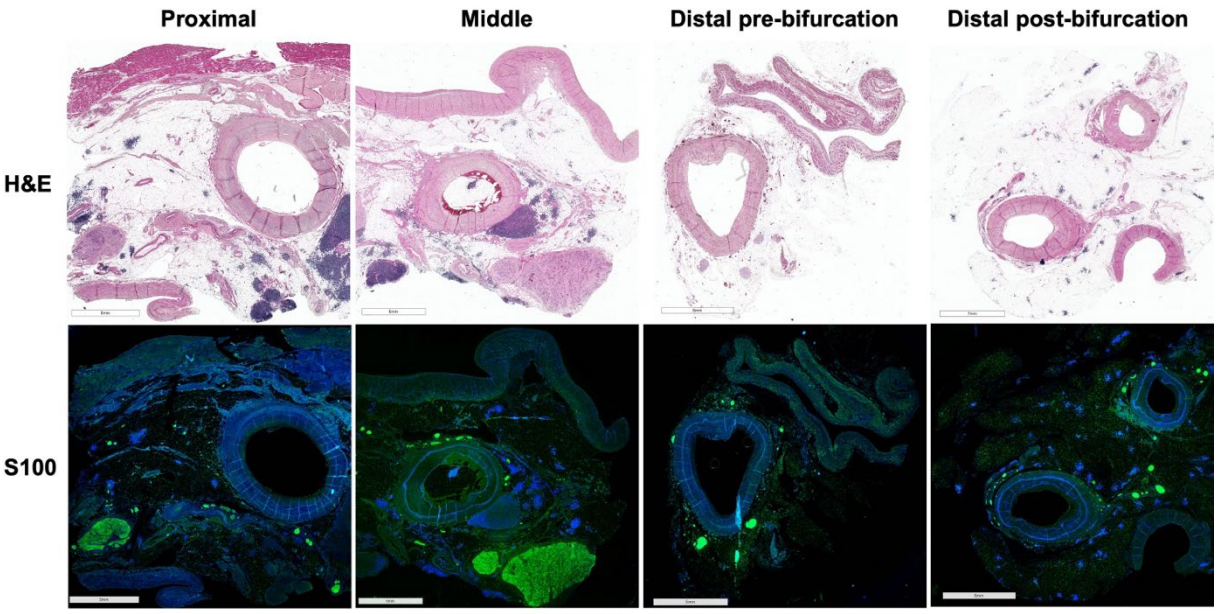

Supplementary Figure 3. Representative images of haematoxylin and eosin (H&E)- and S100-stained slides of different renal artery segments.